Laboratory Investigation (2019) 99:1749–1765
https://doi.org/10.1038/s41374-019-0279-9

TECHNICAL REPORT

Wisteria floribunda agglutinin staining for the quantitative assessment of cardiac fibrogenic activity in a mouse model of dilated cardiomyopathy

Chiaki Nagai-Okatani[1] · Mitsuhiro Nishigori[2] · Takashi Sato[1] · Naoto Minamino[2] · Hiroyuki Kaji[1] · Atsushi Kuno[1]

Received: 8 January 2019 / Revised: 24 April 2019 / Accepted: 10 May 2019 / Published online: 28 June 2019

Abstract

Cardiac fibrosis is a typical phenomenon in failing hearts for most cardiac diseases, including dilated cardiomyopathy (DCM), and its specific detection and quantification are crucial for the analysis of cardiac remodeling. Since cardiac fibrosis is characterized by extensive remodeling of the myocardial extracellular matrix (ECM), in which glycoproteins are the major components, we assumed that fibrosis-related alterations in the cardiac glycome and glycoproteome would be suitable targets for the detection of cardiac fibrosis. Here, we compared protein glycosylation between heart tissues of normal and DCM model mice by laser microdissection-assisted lectin microarray. Among 45 lectins, *Wisteria floribunda* agglutinin (WFA) was selected as the most suitable lectin for staining cardiac fibrotic tissues. Although the extent of WFA staining was highly correlated ($r > 0.98$) with that of picrosirius red staining, a common collagen staining method, WFA did not bind to collagen fibers. Further histochemical analysis with *N*-glycosidase revealed that WFA staining of fibrotic tissues was attributable to the binding of WFA to *N*-glycoproteins. Using a mass spectrometry-based approach, we identified WFA-binding *N*-glycoproteins expressed in DCM hearts, many of which were fibrogenesis-related ECM proteins, as expected. In addition, the identified glycoproteins carrying WFA-binding *N*-glycans were detected only in DCM hearts, suggesting their cooperative glycosylation alterations with disease progression. Among these WFA-binding ECM *N*-glycoproteins, co-localization of the collagen α6(VI) chain protein and WFA staining in cardiac tissue sections was confirmed with a double-staining analysis. Collectively, these results indicate that WFA staining is more suitable for the quantitative assessment of cardiac fibrogenic activity than current collagen staining methods. Furthermore, given that plasma WFA-binding glycoprotein levels were significantly correlated with the echocardiographic parameters for left ventricular remodeling, cardiac WFA-binding glycoproteins are candidate circulating glyco-biomarkers for the quantification and monitoring of cardiac fibrogenesis.

Introduction

Dilated cardiomyopathy (DCM), defined by the presence of left ventricular (LV) dilatation and contractile dysfunction, is one of the most common causes of heart failure [1], with an incidence of >36.5 cases per 100,000 people [2]. Owing to its poor prognosis, with a 5-year survival rate of ~50% after diagnosis [3], DCM is the most common indication for heart transplantation worldwide [1]. For the timely and precise management of DCM patients, and especially for the prevention of sudden cardiac death, accurate risk stratification is of paramount importance [4]. Recent studies show the clinical value of the assessment of cardiac remodeling for risk stratification of DCM [5–7].

Supplementary information The online version of this article (https://doi.org/10.1038/s41374-019-0279-9) contains supplementary material, which is available to authorized users.

✉ Chiaki Nagai-Okatani
chiaki-okatani@aist.go.jp

✉ Atsushi Kuno
atsu-kuno@aist.go.jp

[1] Glycoscience and Glycotechnology Research Group, Biotechnology Research Institute for Drug Discovery, National Institute of Advanced Industrial Science and Technology, Tsukuba, Ibaraki, Japan

[2] Omics Research Center, National Cerebral and Cardiovascular Center, Suita, Osaka, Japan

Cardiac remodeling is the adaptive response of cellular and extracellular compartments of the heart to mechanical or hormonal activation, leading to changes in the shape, volume, and mass of the LV, and is often accompanied with fibrosis [8]. Cardiac fibrosis is characterized by the net accumulation of extracellular matrix (ECM) components, including collagen, and contributes directly or indirectly to both systolic and diastolic dysfunction in numerous cardiac pathophysiologic conditions [9]. Based on the morphological profiles, cardiac fibrosis can be classified into two types: a focal type (also referred to as replacement fibrosis), with replacement of dead cardiomyocytes and scar formation; and a diffuse type (also referred to as reactive fibrosis), which occurs in the interstitial and perivascular spaces without notable cell loss [9, 10]. The latter type of cardiac fibrosis is the major one observed in DCM [1].

Since cardiac fibrosis is a typical phenomenon of failing hearts with most cardiac diseases, including DCM, its quantification is crucial for evaluating cardiac remodeling. In current clinical practice, late gadolinium-enhanced cardiac magnetic resonance is typically used for the assessment of cardiac fibrosis [5–7, 11]. However, the current cardiac magnetic resonance-based assessment is essentially qualitative and not quantitative. Alternatively, chromogenic staining methods are still commonly used for the quantification of cardiac fibrosis in tissue specimens, using dyes such as Masson's trichrome (MT) and picrosirius red (PSR) [12, 13] that stain collagen fibers consisting mostly of type I and III collagens [14]. However, it has been shown in patients with DCM that the degree of fibrosis in endomyocardial biopsy specimens quantified by these methods was not correlated with the degree of cardiac remodeling [15, 16]. Regarding cardiac fibrosis markers, although the serum levels of two collagen by-products have been proven to correlate with cardiac fibrosis [17], these biomarkers showed only a weak correlation with the degree of cardiac remodeling [15]. Consequently, a novel method for assessing cardiac fibrosis that estimates both the quantitative and qualitative alterations in ECM components is greatly needed [17].

Since cardiac fibrosis is a major feature of DCM, it is inevitable that alterations in cardiac ECM, along with cardiac remodeling, are involved in the development and progression of this disease [18]. Cardiac ECM is a complex meshwork of fibers in which cardiomyocytes, fibroblasts, and cardiac vascular cells reside, and consists of structural and nonstructural proteins, collectively known as the matrisome [19]. The major structural components are collagens and elastins, whereas the nonstructural ECM components are important modulators of ECM remodeling and can be divided into three major glycoconjugate groups: glycoproteins, proteoglycans, and glycosaminoglycans [20]. Considering that the glycosylation state of glycoproteins is responsible for the regulation of their functions [20], pathological cardiac remodeling is presumed to be associated with alterations in protein glycosylation. Therefore, fibrosis-related alterations in the cardiac glycoproteome, including in ECM glycoproteins, are primary targets for the detection of cardiac fibrosis. However, fibrosis-related glycosylation changes in the cardiac glycoproteomes have yet to be reported.

In this study, to characterize DCM-related alterations in cardiac glycosylation, we compared protein glycosylation in the LVs of normal and 4C30 DCM transgenic model mice. These mice overexpress beta-galactoside alpha-2,3-sialyltransferase 2 (*St3gal2*) and present with DCM symptoms resulting from indirect cardiac functional defects induced by the accumulation of endoplasmic reticulum stress [21–23]. For this comparison, we performed a laser microdissection (LMD)-assisted lectin microarray (LMA) analysis of formalin-fixed paraffin-embedded (FFPE) cardiac sections [24, 25]. Using this LMD–LMA analysis and subsequent histochemical analyses, we successfully identified *Wisteria floribunda* agglutinin (WFA) as the most suitable lectin for the detection and quantification of cardiac fibrosis. Since the fibrosis-specific WFA staining did not overlap with staining signals of major collagen fiber components, indicating that collagen fibers themselves would not be WFA ligands, we next used mass spectrometry (MS) to identify the WFA-binding (WFA^+) glycoproteins [25, 26]. We also performed a double-staining analysis using WFA and an antibody against one of the identified WFA^+ ECM glycoproteins to verify its WFA staining in cardiac sections. Furthermore, we also evaluated the possibility of using the circulating WFA^+ glycoprotein levels as biomarkers for cardiac fibrosis and the associated cardiac remodeling and dysfunction.

Materials and methods

Animals

The 4C30 mice were provided by Dr. Suzuki and Dr. Matsuda from the Laboratory of Animal Models of the National Institutes of Biomedical Innovation, Health, and Nutrition (NIBIOHN), Osaka, Japan [21]. All animal experiments were performed at the National Cerebral and Cardiovascular Center (NCVC) in accordance with relevant guidelines and regulations and were approved by the Institutional Animal Care and Use Committees at NCVC. All animals were bred and housed in separate cages, with a maximum of five animals per cage, in a room maintained at 23–25 °C, with a 12-h light and 12-h dark cycle and with ad libitum access to food and water.

Echocardiography

Before tissue collection, the cardiac function of each mouse was evaluated by echocardiography using a Vevo 2100 system (VisualSonics, Toronto, Canada) with an MS400 transducer and M-mode imaging. Mice were sedated by isoflurane inhalation (3%) via a nose cone during the procedure.

Tissue section preparation

FFPE tissue sections were prepared as reported previously [27]. Briefly, 24-week-old male mice were anesthetized and perfused from the LV, with 0.1 M phosphate-buffered saline (PBS) at pH 7.4 for 10 min and then with 4% paraformaldehyde in PBS for 10 min. Heart tissues collected from the mice were fixed with 4% paraformaldehyde in PBS for 24 h at room temperature (RT) and then embedded in paraffin. Horizontal sections (5-μm thick) were prepared from the resultant FFPE blocks, mounted on poly-L-lysine-coated polyethylene naphthalate-membrane glass slides (Leica Microsystems, Wetzlar, Germany) for LMD–LMA analyses; for histochemical analyses, 2-μm-thick horizontal sections were prepared. Brain sections were prepared as described above, using normal 8-week-old mice. Coronal cardiac sections (2-μm thick) of 24-week-old mice were prepared from the fixed tissues, using the PAXgene tissue fixation system (PreAnalytiX, Hombrechtikon, Switzerland), according to the manufacturer's instruction; this system was used, because it allowed for improved fixation of the dilated morphology of DCM cardiac tissues compared with that of formalin-fixed tissues.

Tissue section staining

All tissue sections were deparaffinized three times with xylene for 5 min each and rehydrated in graded ethanol concentrations. Collagen fibers were stained with MT (Sigma-Aldrich, St. Louis, MO, USA), along with Weigert's iron hematoxylin (Sigma-Aldrich), or with PSR (ScyTek Laboratories, Logan, UT, USA) according to the manufacturers' instructions. The stained sections were mounted with Entellan new (Merck, Darmstadt, Germany). For hematoxylin staining before LMD, the deparaffinized sections were washed with water, stained with Mayer's hematoxylin (Wako, Osaka, Japan), dried, and stored at RT until use. For fluorescent histochemistry, antigen retrieval was performed by autoclaving the sections for 10 min at 110 °C in citrate buffer (pH 6.0; Agilent Technologies, Santa Clara, CA, USA) for staining of collagen alpha-6(VI) (Col6a6) or biotinylated lectins, or Tris-ethylenediaminetetraacetic acid buffer (pH 9.0; Agilent Technologies) for staining of myosin-regulatory light chain 2 (Myl2), a cluster of differentiation 31/platelet endothelial cell-adhesion molecule-1 (Cd31/Pecam1), vimentin (Vim), and collagen alpha-1(I)/alpha-2(I) (Col1a1/Col1a2). After antigen retrieval, all washing steps were performed three times with 10 mM PBS at pH 7.4.

Single lectin staining was performed, using a biotin–streptavidin system, as described previously, with slight modifications [27]. Briefly, after antigen retrieval, the sections were blocked with the streptavidin–biotin blocking kit (Vector Laboratories, Burlingame, CA, USA) and further blocked with a carbo-free blocking solution (Vector Laboratories) for 1 h at 20 °C. The sections were incubated overnight at 4 °C with a biotinylated lectin (2 μg/mL in PBS) purchased from Vector Laboratories (WFA, PSA, MAL-I, LEL, ACA, and MAH; the abbreviations of the lectins used in this study are summarized in Supplementary Table 1) and J-chemical (Tokyo, Japan; LCA and AAL); biotinylated AOL was prepared by biotinylation of AOL lectin (Tokyo Chemical Industry, Tokyo, Japan) using the biotin-labeling kit-NH_2 (Dojindo, Kumamoto, Japan). The sections were further incubated with Alexa Fluor 647-conjugated streptavidin (1 μg/mL in PBS; Thermo Fisher Scientific, Waltham, MA, USA) for 1 h at 20 °C, and then stained with Hoechst 33342 (0.5 μg/mL in PBS; Dojindo) for 20 min at 20 °C. The stained sections were mounted in ProLong Gold antifade reagent (Thermo Fisher Scientific). To evaluate the effects of glycosidases on WFA staining, the deparaffinized sections were incubated with chondroitinase ABC (2 mU/μL; Seikagaku Kogyo, Tokyo, Japan), or peptide-*N*-glycosidase F (PNGase F; 5 U/μL, Takara Bio, Shiga, Japan) for 16 h at 37 °C, and subsequent WFA staining procedures were performed as described above.

For double-fluorescence staining with an antibody and WFA, after deparaffinization and subsequent blocking with carbo-free blocking solution, the sections were separately incubated overnight at 4 °C with the following primary antibodies: Myl2 (1:50; 10906-1-AP; Proteintech, Chicago, IL, USA), Cd31 (1:800; 11265-1-AP; Proteintech), Vim (1:1000; 10366-1-AP; Proteintech), Col1a1/Col1a2 (1:200; ab34710; Abcam, Cambridge, MA, USA), and Col6a6 (MBS535250; MyBioSource, San Diego, CA, USA). The sections were then serially incubated with fluorescein isothiocyanate (FITC)-conjugated WFA (2 μg/mL in PBS; Vector Laboratories) for 4 h at 4 °C, Alexa Fluor 594-conjugated goat anti-rabbit IgG (H + L) secondary antibody (highly cross-absorbed grade; 1 μg/mL in PBS; Thermo Fisher Scientific) for 1 h at 20 °C, and Hoechst 33342 (0.5 μg/mL in PBS; Dojindo). For double-fluorescence staining with WFA and wheat germ agglutinin (WGA), after blocking, the sections were serially incubated with

biotinylated WFA (2 μg/mL in PBS) overnight at 4 °C and FITC-conjugated WGA (2 μg/mL in PBS; Vector Laboratories) for 1 h at 20 °C. To quench the autofluorescence, the stained sections were incubated with the TrueView autofluorescence quenching kit (Vector Laboratories) for 5 min at RT before mounting in the VECTASHIELD hard set mounting medium (Vector Laboratories).

Images of the stained sections were obtained using a fluorescence microscope (BZ-X710; Keyence, Osaka, Japan). The fibrotic area was calculated as the ratio of the PSR-stained area divided by the total area of the horizontal cardiac section stained with PSR, using a measurement software program (hybrid cell count and macro cell count; Keyence). Similarly, the WFA-stained area was calculated as the ratio of the WFA-stained area divided by the WGA-stained area (corresponding to the total area) of the horizontal section that was double-stained with WFA and WGA.

Tissue dissection and protein extraction

Tissue dissection using an LMD system (LMD7000, Leica Microsystems) attached to a microscope (DM6000B, Leica Microsystems) and subsequent protein extraction were performed as described previously, with slight modifications [27]. Briefly, tissue fragments (total area: 0.5 mm^2) from hematoxylin-stained sections were collected into a tube and then heat-denatured in 10 mM citrate buffer at pH 6.0 for 1 h at 95 °C. After centrifugation at 20000 × *g* for 1 min at 4 °C (all the following centrifugation steps were performed similarly), 2 μL of a 25% (w/v) slurry of microcrystalline cellulose (Sigma-Aldrich) in Dulbecco's PBS (D-PBS; Takara Bio) was added. After discarding 190 μL of the supernatant and adding 190 μL of D-PBS, the fragments were subjected to protein extraction by sonication, with 20 μL of D-PBS containing 0.5% Nonidet P-40. After incubation for 1 h on ice followed by centrifugation, the supernatants were collected as protein extracts.

LMA analysis

The LMA procedure was carried out essentially as described previously [27]. Briefly, 20 μL of protein extracts were fluorescently labeled with Cy3-succinimidyl ester (Cy3-SE; 10 μg of protein equivalent; GE Healthcare, Buckinghamshire, UK) for 1 h at RT in the dark. After adjusting the volume to 100 μL with probing buffer (25 mM Tris-HCl at pH 7.5, containing 137 mM NaCl, 2.7 mM KCl, 500 mM glycine, 1 mM $CaCl_2$, 1 mM $MnCl_2$, and 1% Triton X-100), the sample solutions were incubated for 2 h at RT to quench the excess reagent. After appropriate dilution with the probing buffer, the sample solutions (0.075–0.3 mm^2 equivalent) were added to wells (60 μL/well) on the lectin array chip (LecChip; GlycoTechnica, Yokohama, Japan) containing triplicate spots of 45 lectins (Supplementary Table 1). After incubating overnight at 20 °C and washing three times with probing buffer, the array chip was scanned using an evanescent-field fluorescence scanner (GlycoStation Reader 1200; GlycoTechnica). All data were analyzed using GlycoStation Tools Pro Suite 1.5 software (GlycoTechnica). The net intensity was calculated by subtracting the background from the signal intensity. The data under appropriate gain conditions providing net intensities below 40,000 for all spots were used to obtain the glycomic profiles, which were presented as the relative signal intensities of the 45 lectins normalized to the mean value of all the lection signals.

The LMA analysis of plasma samples prepared from anesthetized mice as described previously [23] was performed as follows: plasma was diluted with PBS containing 1% Triton X-100 (PBS-Tx; 8 nL plasma/10 μL), labeled with Cy3-SE (20 μg of protein equivalent), and subjected to LMA analysis (8 nL of plasma equivalent/well) as described above. Similarly, for LMA analysis of LV tissue lysates prepared as described below, lysates were diluted with PBS-Tx (200 ng/10 μL), labeled with Cy3-SE (10 μg of protein equivalent), and subjected to LMA analysis (100 ng of protein equivalent/well). Data were shown as the net intensity.

Tissue lysate preparation

For preparation of tissue lysates, tissue collection was carried out essentially as described previously [23]. Briefly, mice were anesthetized by intraperitoneal injection of pentobarbital (somnopentyl; 50 mg/kg, Kyoritsu Seiyaku, Tokyo, Japan) and perfused from the LV with saline containing heparin (5 U/mL) for 15 min. The LV tissues were then collected, quickly diced, frozen in liquid nitrogen, and stored at −80 °C until use.

Aliquots of the frozen LV tissues of 4C30 and wild-type (WT) mice (~10 mg of wet weight/mouse, $N = 3$/group) were pooled and subjected to cryogenic grinding using a mortar and pestle. The resulting tissue powders were then subjected to protein extraction, with 300 μL of extraction buffer (Cellytic MT Cell Lysis Reagent [Sigma-Aldrich] containing 1% protease inhibitor cocktail [P8340; Sigma-Aldrich]) by pulsed sonication (ON, 10 s; OFF, 10 s) for 15 min with Bioruptor (UCD-200TM; output, high; Cosmo Bio, Tokyo, Japan). After centrifugation at 12000 × *g* for 10 min at 4 °C and collection of the supernatants, the pellets were again subjected to the same protein extraction procedure. The supernatants were then combined and used for tissue extracts, which were quantified using a Micro BCA protein assay kit (Thermo Fisher Scientific).

WFA affinity capture from tissue extracts

Collection of WFA^+ proteins from the LV tissue extracts was performed as follows: first, prewashed FG streptavidin magnetic beads (Tamagawa Seiki, Nagano, Japan) were incubated with biotinylated WFA (10 μg/mg beads) in PBS-Tx to obtain WFA-immobilized beads. Then, 200 μg of the tissue extracts were incubated with 2 mg of the prewashed WFA beads in 500 μL of binding buffer (10 mM HEPES at pH 7.3, containing 150 mM NaCl, 1 mM $CaCl_2$, and 1 mM $MnCl_2$) overnight at 4 °C with shaking, to capture the WFA^+ proteins. After washing three times with the binding buffer, the beads were incubated with elution buffer 1 (10 mM HEPES at pH 7.3, containing 200 mM *N*-acetyl-D-galactosamine [GalNAc] and 150 mM NaCl) overnight at 4 °C with shaking, to obtain the GalNAc elution fractions (2 μg of input equivalent/μL). The beads were then heated with elution buffer 2 (10 mM HEPES at pH 7.3, containing 0.2% (w/v) sodium dodecyl sulfate [SDS] and 150 mM NaCl) for 10 min at 95 °C, to obtain the SDS elution fractions (2 μg of input equivalent/μL). To deplete contaminated biotinylated WFA, the SDS elution fractions were further incubated with new FG streptavidin magnetic beads (20 μg/μL eluate) for 1 h at 4 °C with shaking before analysis. Similar manipulations were also performed with biotinylated bovine serum albumin (BSA) prepared using the biotin-labeling kit-NH_2, to obtain BSA-binding (BSA^+) proteins as the negative control.

Sample preparation for MS analyses

WFA^+ proteins were subjected to *S*-reduction with dithiothreitol (Wako) and alkylation with iodoacetamide (Wako) and then digested with Lys-C endopeptidase (Wako) followed by *N*-tosyl-L-phenylalanyl chloromethyl ketone-treated trypsin (Promega, Madison, WI, USA), as described previously [28]. Each digest was separated by hydrophilic interaction chromatography (HILIC) on a TSKgel Amide-80 column (2.0 mm i.d. × 50 mm; Tosoh, Tokyo, Japan) at a flow rate of 0.2 mL/min with monitoring by absorbance at 215 nm, to obtain the pass-through fraction ($HILIC^-$, passed in 75% acetonitrile containing 0.1% trifluoroacetic acid [TFA]) and the bound fraction ($HILIC^+$, eluted with 50% acetonitrile containing 0.1% TFA). The $HILIC^-$ fraction was analyzed by liquid chromatography coupled with tandem MS (LC–MS/MS) to identify WFA^+ proteins. To identify the *N*-glycosylated sites of WFA^+ proteins, an aliquot of the $HILIC^+$ fraction containing glycopeptides was analyzed by isotope-coded glycosylation site-specific tagging (IGOT)–LC–MS/MS [29], in which the *N*-glycan moiety was removed by digestion with PNGase F (Takara Bio) in $H_2{}^{18}O$ (Taiyo Nippon Sanso, Tokyo, Japan) as described previously [28]. The remaining glycopeptides were further applied for WFA affinity capture using a WFA column (5.0 mm i.d. × 14 mm; agarose-bound WFA, Vector Laboratories) at a flow rate of 0.5 mL/min, with monitoring by absorbance at 230 nm, to obtain WFA^+ glycopeptides, as described previously [30]. After washing with 10 mM HEPES at pH 7.0, containing 1 mM $CaCl_2$ and 1 mM $MnCl_2$, the bound glycopeptides were eluted with 10 mM HEPES (pH 7.0) containing 20 mM GalNAc. The $HILIC^+WFA^+$ fractions were cleaned by reversed-phase LC (solvent, 5% acetonitrile containing 0.1% TFA; eluting solvent, 70% acetonitrile containing 0.1% TFA; flow rate, 0.1 mL/min; absorbance, 215 nm) using a C18 column (2.0 mm i.d. × 50 mm; Mightysil RP-18GP; Kanto Chemical, Tokyo, Japan). The resultant glycopeptides were subjected to IGOT–LC–MS/MS to identify *N*-glycosylation sites in the $HILIC^+WFA^+$ glycopeptides. Similar manipulations and analyses were also performed for BSA^+ proteins as the negative control.

LC–MS/MS analysis

LC–MS/MS measurements and database searches were performed as described previously, with slight modifications [31]. Briefly, peptides of the $HILIC^-$ fraction and PNGase F-treated peptides of the $HILIC^+$ fraction were separated by nanoflow LC (flow rate, 300 nL/min) on a C18 tip column (0.15 mm i.d. × 100 mm, Nikkyo Technos, Tokyo, Japan). The eluate was electrospray ionized and introduced directly into a mass spectrometer (LTQ-Orbitrap Velos ETD, Thermo Fisher Scientific) operated by data-dependent acquisition in positive mode. The MS1 spectra were obtained with an Orbitrap analyzer (resolution, 30,000 at *m/z* 400), and collision-induced dissociation MS2 spectra of ten intense signals (normalized collision energy, 35) were obtained with an ion trap analyzer. The deglycosylated peptides of the $HILIC^+WFA^+$ fraction after PNGase F digestion were separated with a tip column (0.075 mm i.d. × 150 mm, Nikkyo Technos) and analyzed with a mass spectrometer (Orbitrap Fusion, Thermo Fisher Scientific). The MS1 spectra were obtained with an Orbitrap analyzer (resolution, 120,000 at *m/z* 200), and high-energy collision-induced dissociation (stepped collision energy, 30 ± 5). The MS2 spectra were obtained by data-dependent mode (cycle time, 3 s) with the same analyzer (resolution, 15,000 at *m/z* 200).

The mass data were processed on the Proteome Discoverer software (ver. 2.2, Thermo Fisher Scientific), using the Mascot database search engine (ver. 2.5.1, Matrix Science, London, UK) and the Swiss-Prot protein sequence database (16,992 entries for mouse, downloaded in July 2018). The search conditions for non-glycopeptides were as follows: enzyme, trypsin, and Lys-C; maximum missed cleavages, 2;

Table 1 Pathophysiological characteristics of 4C30 and WT mice

	12-week-old		24-week-old	
	WT	4C30	WT	4C30
N	9	9	7	7
HW/BW (%)	0.56 ± 0.05	0.71 ± 0.08*	0.49 ± 0.04	0.83 ± 0.26*
LVDd (mm)	3.33 ± 0.28	4.06 ± 0.42*	3.75 ± 0.23	4.67 ± 0.78*
LVDs (mm)	1.90 ± 0.32	2.90 ± 0.63*	2.34 ± 0.57	4.16 ± 1.09*†
EF (%)	74.8 ± 7.3	55.5 ± 13.7*	66.9 ± 16.5	25.4 ± 18.9*†
FS (%)	43.1 ± 7.3	29.3 ± 10.0*	37.8 ± 12.3	12.2 ± 9.6*†

Data are presented as means ± SD

HW heart weight, *BW* body weight, *LVDd* LV end-diastolic dimension, *LVDs* LV end-systolic dimension, *EF* ejection fraction, *FS* fractional shortening

*$P < 0.05$ between 4C30 and age-matched WT mice

†$P < 0.05$ between 4C30 mice at 12 and 24 weeks

fixed modification, carbamidomethyl Cys; variable modifications, ammonia loss (N-term C), Gln- > pyro-Glu (N-term Q), and oxidation (M); MS1 tolerance, 7 ppm; MS2 tolerance, 0.8 Da for ion trap, 0.02 Da for Orbitrap. In the case for deglycopeptides, Delta:H(1)N(−1)18 O(1) (N) [this is the registered term in UniMod; however, to be precise, it should be Delta:H(−1)N(−1)18 O(1) (N)] was added as a variable modification. The significance threshold was set to 0.05, and if the false discovery rate (FDR) exceeded 1%, a threshold value of 1% or less was used for FDR. For glycopeptide identification, hit peptides (rank = 1 and expectation value ≤ significance threshold), including the aforementioned Asn modification on a consensus sequence for *N*-glycosylation (Asn-Xaa [any amino acid except for Pro]-Ser or Thr or Cys) were selected as *N*-glycopeptides. The proteins identified with at least two peptides were considered as the identified proteins. The presence of signal peptides and transmembrane segments in the identified proteins was predicted using SignalP (ver. 4.1; http://www.cbs.dtu.dk/services/SignalP/), SOSUI (Batch; http://harrier.nagahama-i-bio.ac.jp/sosui/), and TMHMM Server (ver. 2.0; http://www.cbs.dtu.dk/services/TMHMM/), as described previously [31]. Gene Ontology term analyses were performed using DAVID (ver. 6.8; http://david.abcc.ncifcrf.gov) as described previously [31].

WFA blot analysis

WFA blot analyses of the WFA^+ proteins were performed essentially as described previously [32]. Briefly, the GalNAc and SDS elution fractions (20 μg of input equivalent) were separated by SDS–polyacrylamide gel electrophoresis and transferred onto polyvinylidene difluoride membranes (Bio-Rad, Hercules, CA, USA). After blocking with the carbo-free blocking solution for 1 h at RT, the membranes were washed with the binding buffer and then incubated with FITC-conjugated WFA (5 μg/mL in the binding buffer) overnight at 4 °C. After washing with Tris-buffered saline (TBS; 25 mM Tris-HCl at pH 7.5, containing 137 mM NaCl and 2.7 mM KCl) containing 0.1% Tween 20 (TBS-T), the membranes were further incubated with rabbit anti-FITC Fab (1:1000; Dako, Carpinteria, CA, USA) for 1 h at RT. After serial washing with TBS-T and TBS, the chemiluminescence blot was analyzed with a membrane scanner (C-DiGit; LI-COR, Lincoln, NE, USA) using ImmunoStar LD (Wako).

Statistical analysis

Statistical comparison was performed with the Student's unpaired *t* test ($N < 6$/group) or Mann–Whitney's *U* test ($N \geq 6$/group) for two groups, and with the Steel–Dwass test ($N \geq 6$/group) for four groups. The differences were considered significant when $P < 0.05$. Statistical analyses, including a principal component analysis for multivariable data, were performed using the JMP software (ver. 13.2.1; SAS Institute, Cary, NC, USA).

Results

Screening of lectins that recognize characteristic glycans in cardiac fibrotic tissues

The primary objective of this study was to characterize protein glycosylation in fibrotic areas within failing mouse cardiac tissues. For this aim, we first compared the glycomic profiles of cardiac tissues obtained from 4C30 and WT mice. The 4C30 mice exhibited typical features of DCM, including an enlarged LV cavity and a reduced ejection fraction at 12 weeks, and advanced cardiac dysfunction at 24 weeks (Table 1). Thus, FFPE cardiac sections prepared from 24-week-old 4C30 and WT mice were subjected to LMD–LMA analysis as illustrated in Fig. 1a. Since obvious fibrosis was observed within the LV tissues of 4C30 hearts (Fig. 1b), LV

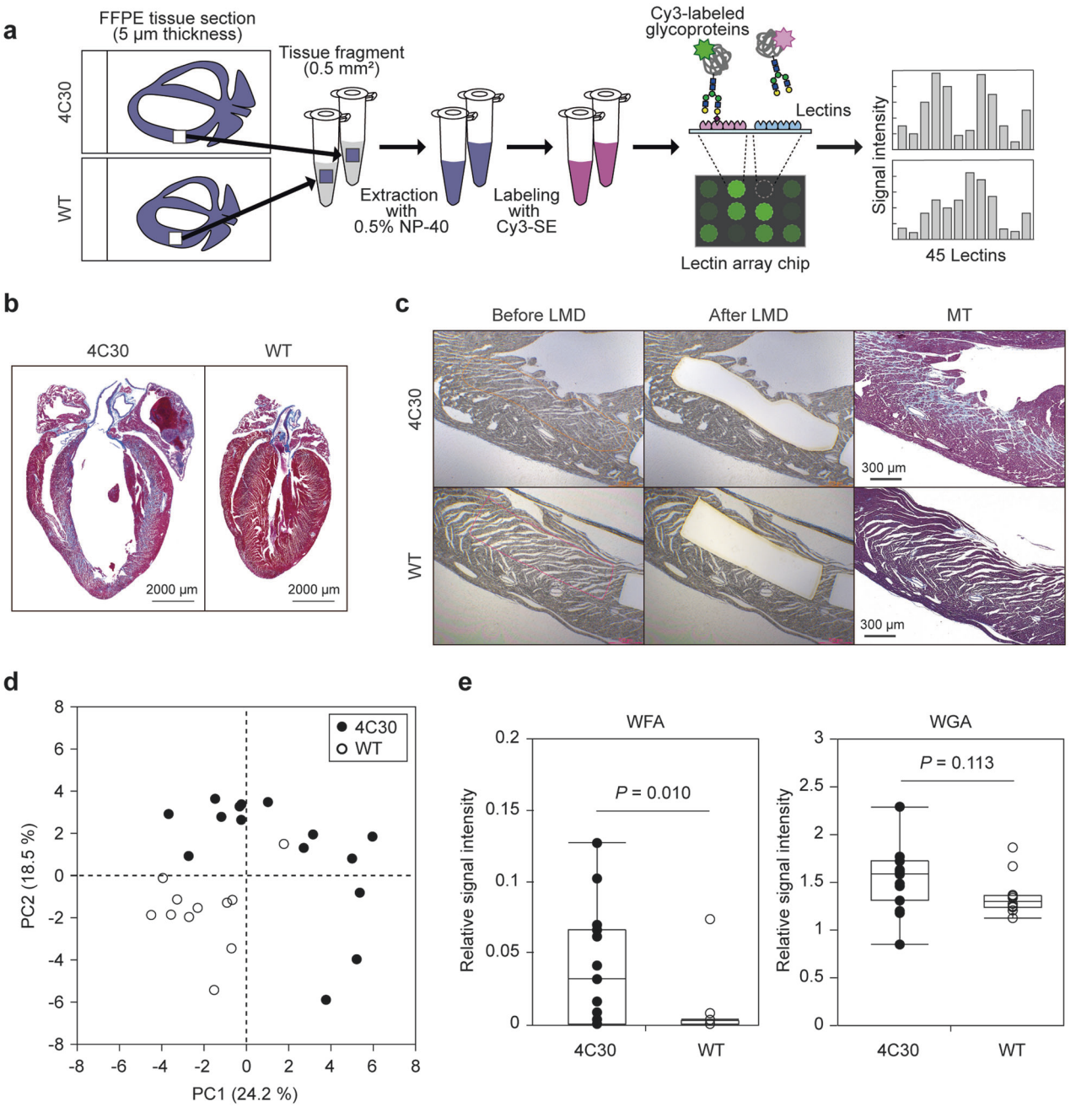

Fig. 1 Differential glycomic profiling of cardiac sections obtained from 4C30 and WT mice. **a** Schematic overview of the LMD–LMA analysis. In brief, tissue fragments were obtained from a hematoxylin-stained FFPE cardiac section by LMD and then subjected to protein extraction. The resultant protein mixtures were labeled with Cy3-SE and then subjected to LMA analysis. Here, the interactions of glycoprotein samples with 45 lectins immobilized on a lectin array chip (Supplementary Table 1) were quantified by their fluorescence intensities, and the resulting glycomic profiles obtained for the 4C30 and WT mice were statistically compared. **b** Cardiac sections from 4C30 and WT mice stained with MT. **c** Representative images before or after tissue dissection (0.5 mm^2 each; left and middle panels) and their corresponding areas in the serial sections stained with MT (right panels). Whole-section images before or after tissue dissection and their MT-stained serial sections are shown in Supplementary Fig. 1. **d** A score plot of principal component analysis showing the differences in the glycomic profiles of the LV tissue fragments ($N = 15$ for 4C30; $N = 12$ for WT) from 4C30 and WT hearts ($N = 3$ mice/group). **e** Comparison of the relative WFA and WGA signal intensities between the 4C30 and WT groups. The *P*-values of Mann–Whitney's *U* tests are indicated. The glycomic profile data used for the analyses shown in (**d**) and (**e**) are presented in Supplementary Table 2

tissue fragments were collected from coronal sections of 4C30 and WT hearts (Fig. 1c; Supplementary Fig. 1). The principal component analysis score plot clearly showed a discrete distribution of the resultant glycomic profiles between the 4C30 and WT groups (Fig. 1d), highlighting the aberrant protein glycosylation within 4C30 failing hearts.

To identify the most suitable lectin for detection of characteristic glycan structures in 4C30 hearts, we statistically compared the relative signal intensity of each lectin obtained from the LMD–LMA analysis between the 4C30 and WT groups (Supplementary Table 2). As a result, the 4C30 samples showed significantly higher signals ($P < 0.05$) for nine lectins, including fucose-binding lectins (PSA, LCA, AOL, and AAL) and a lectin recognizing α2,3-linked sialic acids (MAL-I), a polylactosamine-binding lectin (LEL), several *O*-glycan binders (ACA and MAH), and a lectin recognizing terminal GalNAc (WFA). In contrast, significantly lower signals ($P < 0.05$) were observed for six lectins in the 4C30 samples, including three lectins recognizing α2,6-linked sialic acids (SNA, SSA, and TJA-I), one lectin recognizing galactosylated *N*-glycans (RCA120), and two *O*-glycan binders (Jacalin and HPA). Notably, among these 15 lectins, only WFA exhibited a greater than twofold change between the two groups. The WFA signals of most WT samples were nearly undetectable, in contrast to those of WGA, a plasma membrane-staining lectin (Fig. 1e) [33]. Accordingly, these results suggested that WFA was the most promising candidate as a probe for the detection of aberrant glycosylation in cardiac fibrotic tissues.

Identification of WFA as a lectin probe for cardiac fibrosis-specific staining

To characterize the distribution of carbohydrate ligands for WFA in cardiac fibrotic tissues, a comparative histochemical analysis of FFPE cardiac sections of 4C30 and WT mice was performed. In brief, using serial sections, the distribution of collagen fibers detected by MT staining in one section was compared with the staining patterns of WFA, as well as the other eight lectins that showed a higher signal intensity in the LMD–LMA analysis (Supplementary Fig. 2). The results showed LEL and MAH staining throughout the cardiac tissues of both 4C30 and WT mice. The six lectins, namely, PSA, LCA, AOL, AAL, MAL-I, and ACA, showed relatively strong staining in the fibrotic areas within the LV tissues of 4C30 mice, but the staining was also observed in normal tissues of the 4C30 and WT mice. Notably, in contrast to these lectins, strong WFA staining was observed in the fibrotic areas of the medial half of the LV, whereas WFA staining was observed only in very limited areas of the tissues of WT mice. These analyses demonstrated that WFA was the best lectin probe for the specific staining of fibrotic areas, consistent with the results of the LMD–LMA analysis.

We further compared the distribution of WFA ligands with that of collagen fibers observed in MT- and PSR-stained serial sections, and found that the WFA staining pattern highly resembled the localization pattern of collagen fibers in the LV tissues of 4C30 mice (Fig. 2a). We then compared the ratios of WFA- and PSR-stained areas between the 4C30 and WT mice; these ratios were determined by imaging analyses of serial horizontal sections separately stained with WFA and PSR. Similar to the observations of the coronal sections, the distribution of the staining signals of WFA and PSR resembled each other, with staining being predominantly observed in the inner region of the LV posterior walls of 4C30 hearts (Supplementary Fig. 3). The imaging analyses revealed that the ratios of the fibrotic and WFA-stained areas were significantly higher in 4C30 hearts than in WT hearts (Fig. 2b, c), and these ratios showed a highly positive correlation (Fig. 2d). Taken together, these results indicated that WFA staining was a reliable method for the quantification of cardiac fibrosis.

Characterization of cardiac WFA staining

Notably, no WFA staining was observed in several perivascular regions of the WT hearts, where collagen deposition was observed using the MT and PSR staining methods (Fig. 2a); this suggests that the specific WFA staining of fibrotic areas was not attributable to WFA binding to collagen fibers. We further investigated the localization of WFA staining in cardiac fibrotic tissues by double-staining analyses, using 4C30 heart sections separately stained for various cell markers, followed by WFA staining. As expected, WFA staining did not co-localize with Col1a1 and Col1a2, the major components of collagen fibers (Fig. 3). Similarly, WFA staining did not overlap with that of Myl2, Cd31, and Vim, indicating that the WFA ligands responsible for the extensive WFA staining were not localized in cardiomyocytes, endothelial cells, or fibroblasts. The WFA ligands were instead observed in interstitial regions, suggesting that the extensive WFA staining was a result of WFA binding to several ECM proteins.

Since WFA has a relatively broad carbohydrate specificity [34], candidate WFA ligands include both *N*- and *O*-glycans on glycoproteins, as well as glycosaminoglycans, such as chondroitin sulfate (CS) and dermatan sulfate (DS) on proteoglycans. Thus, we next aimed to determine which glycan type was responsible for the extensive WFA staining observed in cardiac fibrotic tissues by employing glycosidases. We found that the WFA staining pattern in cardiac fibrotic tissues was not altered by pretreatment with chondroitinase ABC, which digests CS and DS (Fig. 4). In contrast, the WFA staining observed at the CS-rich perineuronal net of mouse brain sections [35] was abolished by this glycosidase treatment (Supplementary Fig. 4). These results indicated that CS and DS were not likely candidates. Similarly, we also evaluated the effects of *N*-glycosidase

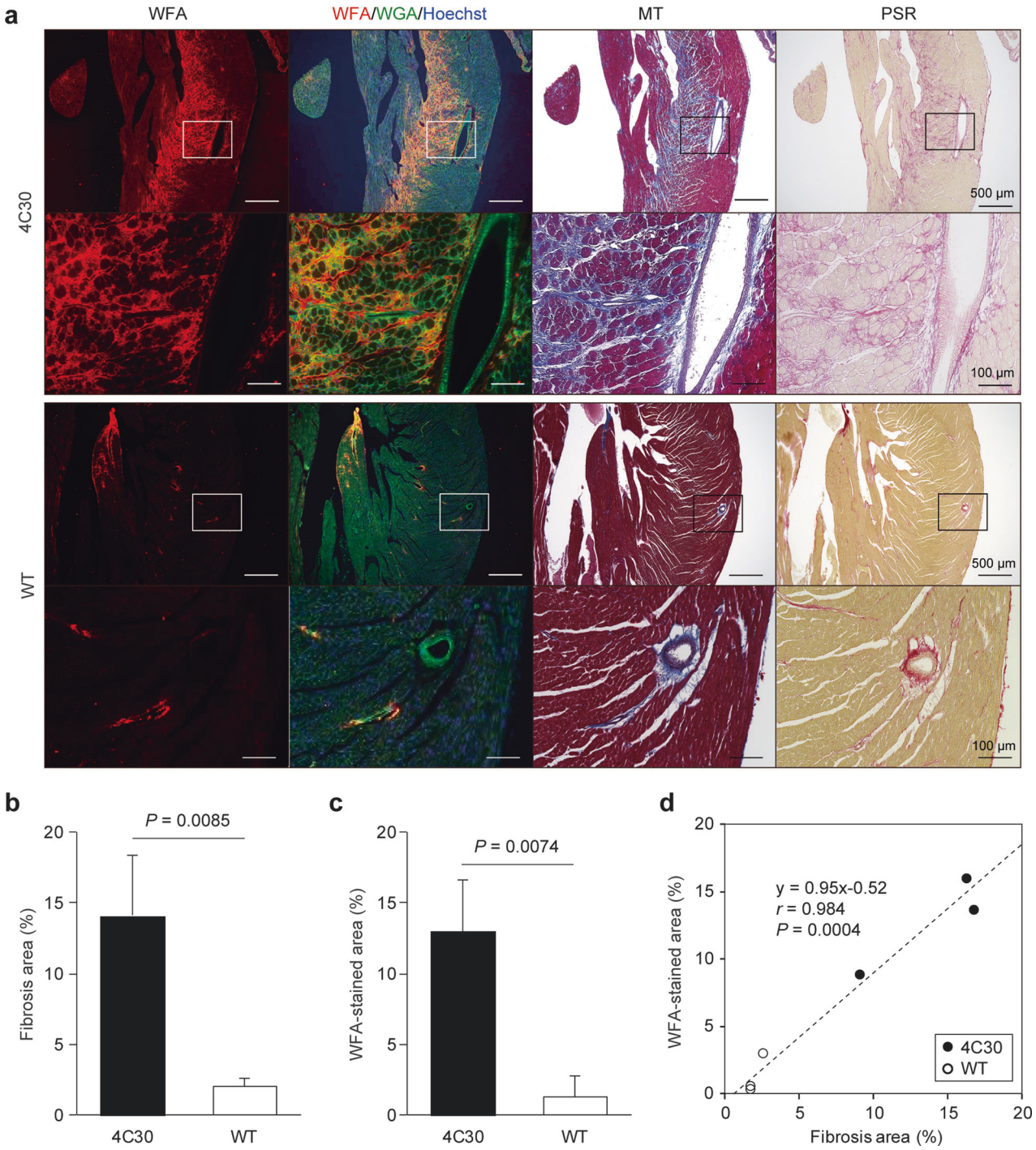

Fig. 2 Histochemical staining of cardiac sections of 4C30 and WT mice. **a** Three serial coronal sections of cardiac tissues obtained from 4C30 and WT mice were separately subjected to MT and PSR staining, and triple fluorescence staining for WFA (red), WGA (green), and Hoechst 33342 (blue). Upper panels for each group are representative images at the same area around LV vessels. Lower panels are enlarged images of the areas indicated in the upper panels. **b–d** The ratios of fibrotic areas (**b**) and WFA-stained areas (**c**) observed in serial horizontal cardiac sections of the two groups ($N = 3$ mice/group) and their correlation (**d**). Pearson's linear correlation coefficient (r) and P-value are indicated. Whole-section images used for these analyses are presented in Supplementary Fig. 3

PNGase F on cardiac WFA staining, and showed that the extensive WFA staining was almost completely abolished by PNGase F treatment (Fig. 4). These results demonstrated that the WFA staining observed in the fibrotic area was mainly attributable to the binding of WFA to *N*-glycoproteins expressed in cardiac fibrotic tissues.

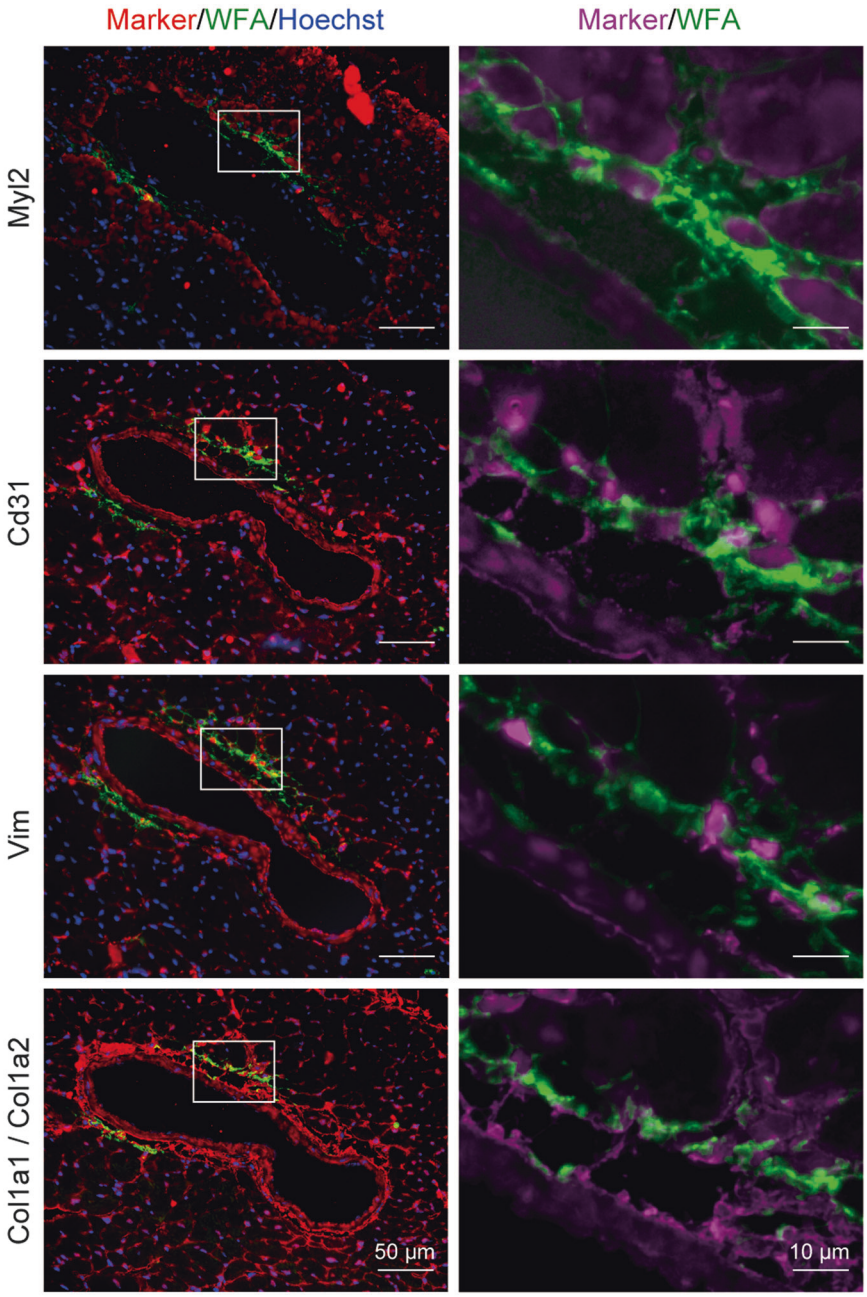

Fig. 3 Fluorescence staining of failing cardiac tissues with WFA and various molecular markers. Serial cardiac sections of 4C30 mice were stained separately with antibodies against Myl2 (ventricular cardiomyocyte marker), Cd31 (endothelial cell marker), Vim (fibroblast marker), and Col1a1/Col1a2 (major components of collagen fibers), and then stained with WFA. Left panels are fluorescence images of the perivascular regions of the triple-stained LV tissues for the indicated molecular marker (red), WFA (green), and Hoechst 33342 (blue). Right panels are enlarged images of the double staining for the marker (magenta) and WFA (green) at the indicated areas in the left panels. Scale bars, 50 μm

Identification of cardiac ECM proteins carrying WFA$^+$ *N*-glycans

Based on the results obtained from histochemical analyses, *N*-glycosylated ECM proteins expressed in cardiac fibrotic tissues were the most likely candidates responsible for the fibrosis-specific WFA staining. Thus, to identify WFA$^+$ cardiac *N*-glycoproteins in 4C30 mice, the following six protein fractions were obtained by the workflow indicated in Fig. 5a: 4C30/WFA/GalNAc, 4C30/WFA/SDS, WT/WFA/GalNAc, WT/WFA/SDS, 4C30/BSA/GalNAc, and 4C30/BSA/SDS. The successful collection of WFA$^+$ proteins by WFA affinity capture was confirmed by WFA blot analysis, in which WFA$^+$ proteins were more abundant in the 4C30/WFA samples than in the WT/WFA samples, as expected (Supplementary Fig. 5). A total of 4823 peptides derived from 390 proteins were identified as major WFA$^+$ or BSA$^+$ proteins from the LC–MS/MS analyses of tryptic digests (HILIC$^-$ fractions) obtained from these six protein samples (Supplementary Table 3). We then selected WFA$^+$ ECM *N*-glycoproteins using the workflow summarized in Supplementary Fig. 6. In brief, we first evaluated whether the 390 identified proteins have potential *N*-glycosylation sites. We also assessed whether signal peptides

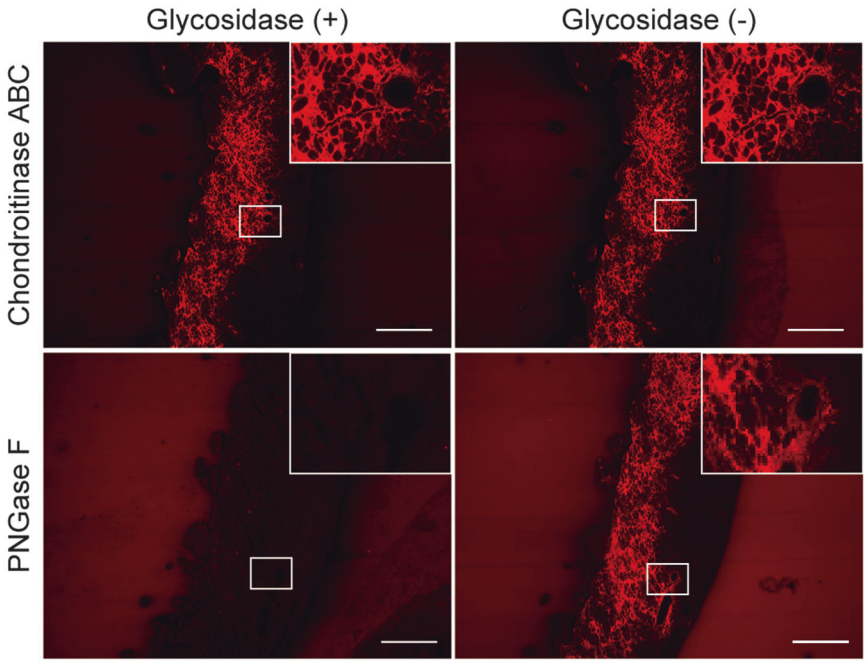

Fig. 4 Effects of glycosidases on WFA staining for failing cardiac tissues. Coronal sections of 4C30 hearts were pretreated with (+) or without (–) chondroitinase ABC or PNGase F and then stained with WFA. Insets are enlarged images of the indicated areas. Scale bars, 500 μm

and potential transmembrane segments were present, and proteins that have neither signal peptides nor transmembrane segments were excluded as candidates, as they were unlikely to be subjected to *N*-glycosylation in vivo. Accordingly, a total of 66 proteins were selected, 24 of which were identified from the 4C30/WFA samples but not from the 4C30/BSA (negative control) samples (Fig. 5b and Supplementary Table 3). Thus, we considered these 24 proteins as plausible major WFA^+ proteins expressed in 4C30 LV tissues.

Because 13 of the 24 selected WFA^+ proteins were fibrogenesis-related ECM proteins based on a Gene Ontology term analysis (Table 2), we further evaluated whether these 13 ECM proteins were *N*-glycosylated. In a list of identified $HILIC^+$ *N*-glycopeptides (505 *N*-glycopeptides derived from 177 *N*-glycoproteins; Supplementary Table 4), one or more *N*-glycosylation sites were identified in 12 of the proteins, except for Mfap5 (Table 2). Similarly, we also checked whether these 13 ECM proteins possessed WFA^+ *N*-glycans. By referring to a list of identified $HILIC^+WFA^+$ *N*-glycopeptides (44 *N*-glycopeptides derived from 24 *N*-glycoproteins; Supplementary Table 5), we confirmed that 7 of the 13 ECM proteins (i.e., Lamc1, Lamb1, Hspg2, Bgn, Lama4, Col6a6, and Postn) were modified by WFA^+ *N*-glycans (Table 2). In contrast, among the remaining 11 non-ECM proteins (i.e., Cdh13, Itgb1, Cdh2, Cox6a2, Bcl2l13, Cd151, Cd200, Cd81, Cyb5b, Atp12a, and Grn), only Itgb1 was identified in the $HILIC^+WFA^+$ fractions. Importantly, 21 of 23 proteins that result in the WFA^+ *N*-glycopeptides identified in the 4C30/WFA sample were ECM proteins (Supplementary Table 6). Moreover, these WFA^+ ECM *N*-glycopeptides were detected in the 4C30/WFA samples but not in the WT/WFA samples (Supplementary Table 5), implying the cooperative altered glycosylation of these glycoproteins. Collectively, these results support that the fibrosis-specific WFA staining was mainly attributable to WFA binding to ECM proteins carrying WFA^+ *N*-glycans.

Verification of the contribution of WFA^+ ECM *N*-glycoproteins to cardiac fibrosis-specific WFA staining

Because collagen VI, an unusual member of the collagen family, is known to interact with collagen protein constituents of collagen fibers [36], we evaluated whether Col6a6 was stained with WFA in cardiac sections by a double-staining analysis. Cardiac sections of 4C30 mice were first stained for Col6a6 and then for WFA. We found that Col6a6 expression was observed throughout the 4C30 cardiac tissues, including both interstitial and perivascular regions, and a small quantity of Col6a6 co-localized with the WFA staining (Fig. 6). These results demonstrated that Col6a6 contributed to cardiac WFA staining, and suggested that the WFA staining was due to WFA binding to multiple *N*-glycoproteins expressed in the cardiac fibrotic tissues, as expected based on the MS analyses.

Evaluation of the disease-related alteration of plasma WFA^+ glycoprotein levels

The MS-based analyses revealed that the expression of multiple soluble WFA^+ *N*-glycoproteins was increased in

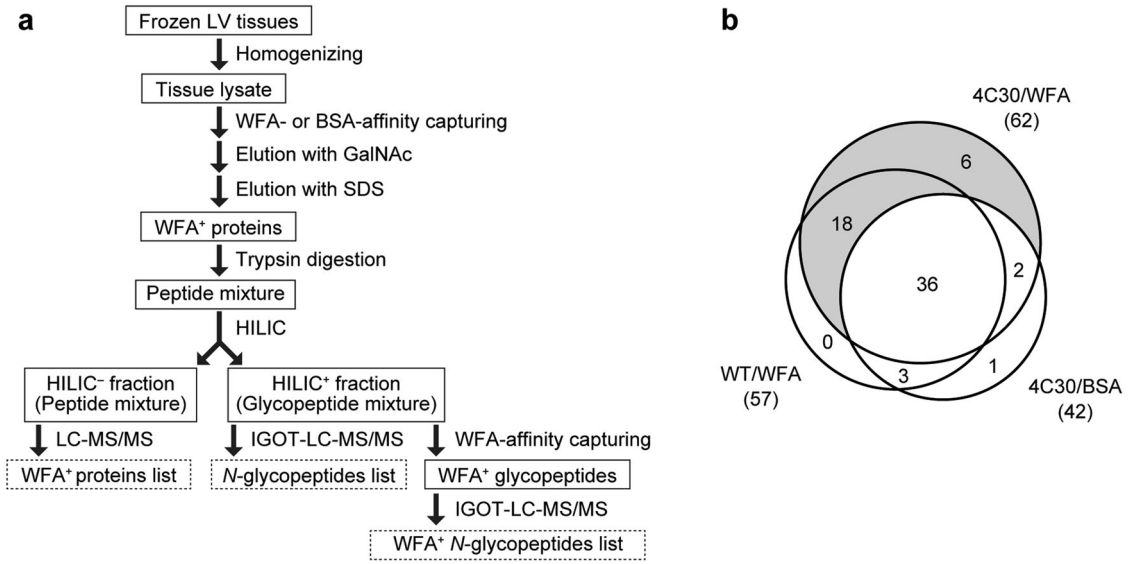

Fig. 5 MS-based identification of WFA$^+$ *N*-glycoproteins in LV tissues. **a** Schematic overview of the present strategy. LV tissues were mixed and homogenized to obtain tissue lysates that were subjected to affinity capture using WFA. As a control, a similar manipulation was performed with BSA to obtain BSA$^+$ proteins. WFA$^+$ proteins were collected by serial elution with GalNAc and subsequent SDS solutions and then subjected to trypsin digestion. The resulting peptide mixture was separated by HILIC to obtain the bound (+) and unbound (–) fractions. The HILIC$^-$ fraction was analyzed to identify major WFA$^+$ proteins by LC–MS/MS. The HILIC$^+$ fraction was partly analyzed by IGOT–LC–MS/MS to determine the *N*-glycosylation sites of the WFA$^+$ proteins. An aliquot of the HILIC$^+$ fraction was also subjected to WFA affinity-based separation to obtain WFA$^+$ glycopeptides, which were analyzed by IGOT–LC–MS/MS to identify WFA$^+$ *N*-glycopeptides. The proteins identified in the HILIC$^+$ or HILIC$^+$WFA$^+$ fractions, but not in HILIC$^-$ proteins, were considered as minor *N*-glycoproteins. **b** Venn diagram illustrating the distribution of 66 WFA$^+$ and BSA$^+$ *N*-glycoproteins identified from 4C30 and WT mice. The total number of identified proteins for each group is indicated in each parenthesis. A total of 24 proteins (highlighted in gray) were detected in the WFA$^+$ sample, but not the BSA$^+$ sample, of 4C30 mice

fibrotic failing hearts, suggesting that circulating levels of these glycoproteins were also elevated. To evaluate this hypothesis, the plasma levels of WFA$^+$ glycoproteins in 4C30 and age-matched WT mice were compared by LMA analysis, in which the WFA signal intensity quantitatively reflects the WFA$^+$ protein concentration. As expected, the plasma levels of WFA$^+$ glycoproteins were significantly higher in 4C30 mice than in age-matched WT mice, both at 12 and 24 weeks (Fig. 7a; Supplementary Table 7). In addition, the plasma concentrations of WFA$^+$ glycoproteins were higher in 24-week-old 4C30 mice than in 12-week-old 4C30 mice, suggesting that the increased levels of WFA$^+$ glycoproteins were associated with DCM progression. At 24 weeks of age, the WFA$^+$ glycoprotein levels in plasma samples were highly positively correlated with those in LV tissue lysates (Fig. 7b; Supplementary Table 8). We also evaluated the correlation of plasma WFA$^+$ glycoprotein levels with echocardiographic parameters, and found that moderate, but significant, correlations existed between the indexes of LV remodeling (LV end-diastolic/systolic diameters) and LV function (ejection fraction and fractional shortening) (Fig. 7c). These results suggested that circulating levels of cardiac WFA$^+$ glycoproteins may be candidate biomarkers that reflect the degree of cardiac remodeling and the associated cardiac dysfunction.

Discussion

In this study, we identified WFA as a suitable lectin for the specific staining of fibrotic cardiac tissues. The utility of the WFA staining was evaluated by comparison with PSR staining, a commonly used method for the detection of established collagen fibers. The WFA staining method could detect the fibrogenic areas of failing hearts, via WFA binding mainly to fibrogenesis-related ECM *N*-glycoproteins expressed in fibrotic cardiac tissues. Importantly, WFA staining could discriminate the disease-relevant fibrosis observed in failing hearts of DCM mice from the collagen deposition in healthy hearts of normal mice. Accordingly, WFA staining enables the quantitative assessment of cardiac fibrogenic activity and may therefore be useful for the monitoring and prognosis of cardiac remodeling and the associated cardiac dysfunction, which was not possible using the current collagen staining methods.

Based on the carbohydrate specificity of WFA, which failed to bind to sialylated glycans [34], the present results suggest that sialylated glycan levels are reduced in the cardiac glycoproteome of 4C30 mice. DCM model mice overexpress St3gal2 [21], which mediates the transfer of sialic acid via a 2,3-linkage to the galactose residue of

Table 2 The summary of WFA^+ ECM proteins identified from the LV tissues of 4C30 mice

Entry name	Gene name	Protein description	No. of identified peptides				No. of identified *N*-glycosylated sites			
			GalNAc elution		SDS elution		$HILIC^{+a}$		WFA^{+b}	
			4C30	WT	4C30	WT	4C30	WT	4C30	WT
LAMC1_MOUSE	*Lamc1*	Laminin subunit gamma-1	47	33	20	9	4	9	2	0
LAMB2_MOUSE	*Lamb2*	Laminin subunit beta-2	40	18	9	4	3	3	0	0
LAMB1_MOUSE	*Lamb1*	Laminin subunit beta-1	25	22	4	5	5	9	1	0
NID1_MOUSE	*Nid1*	Nidogen-1	12	12	3	0	1	1	0	0
PGBM_MOUSE	*Hspg2*	Basement membrane-specific heparan sulfate proteoglycan core protein	1	0	12	5	4	9	1	0
PGS2_MOUSE	*Dcn*	Decorin	11	5	3	0	2	3	0	0
PGS1_MOUSE	*Bgn*	Biglycan	4	0	3	0	2	2	2	0
LAMA4_MOUSE	*Lama4*	Laminin subunit alpha-4	2	3	1	1	1	8	1	0
FBN2_MOUSE	*Fbn2*	Fibrillin-2	0	0	3	1	1	0	0	0
CO6A6_MOUSE	*Col6a6*	Collagen alpha-6(VI) chain	0	0	3	0	6	9	1	0
MFAP5_MOUSE	*Mfap5*	Microfibrillar-associated protein 5	0	0	3	1	0	0	0	0
CATD_MOUSE	*Ctsd*	Cathepsin D	2	1	0	0	1	1	0	0
POSTN_MOUSE	*Postn*	Periostin	0	0	2	0	1	1	1	0

[a]The list of glycopeptides and their N-glycosylation sites identified from $HILIC^+$ fractions is indicated in Supplementary Table 4

[b]The list of glycopeptides and their N-glycosylation sites identified from $HILIC^+WFA^+$ fractions is indicated in Supplementary Table 5

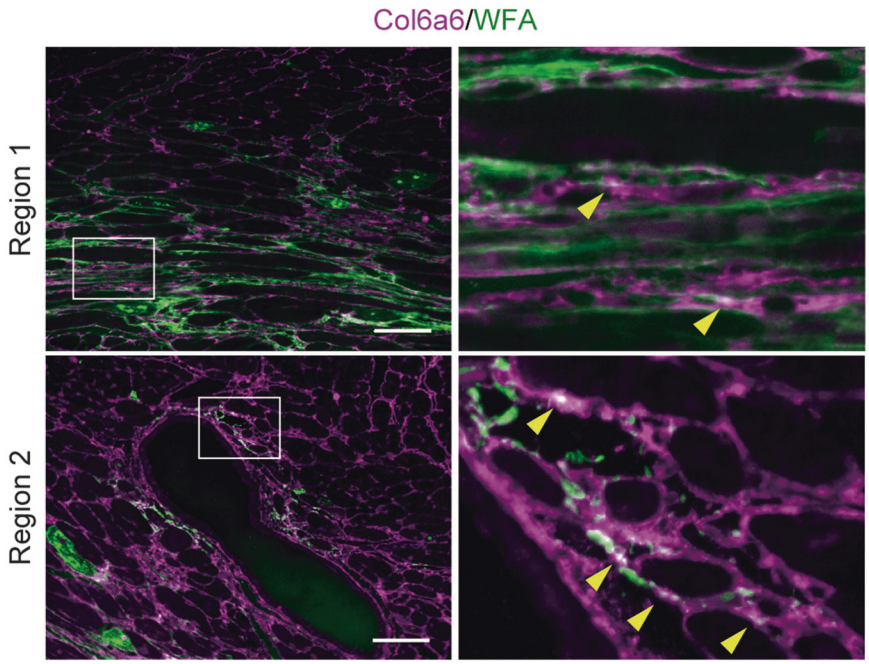

Fig. 6 Double-fluorescence staining for WFA and Col6a6. Left panels are representative merged images of a double-staining analysis for Col6a6 (magenta) and WFA (green) at the interstitial region (Region 1) and perivascular region (Region 2). Right panels are enlarged images of the areas indicated in the left panels. Arrowheads indicate representative double-positive regions shown as white in the merged images. Scale bars, 50 µm

terminal Galβ1,3GalNAc structures on *O*-linked oligosaccharides [37]. In contrast to St3gal2 catalytic activity, decreased sialylation of cardiac-soluble proteins in this model has been suggested by lectin blot analyses, using MAL-I, a α2,3-linked sialic acid-binding lectin, and PNA, an asialo *O*-glycan binder [21]. Therefore, the present results were highly consistent with the previously observed alterations in cardiac protein glycosylation in 4C30 mice, occurring as a consequence of DCM progression rather than St3gal2 overexpression.

Similar to this study, it has been demonstrated that WGA staining is a suitable method for the detection and

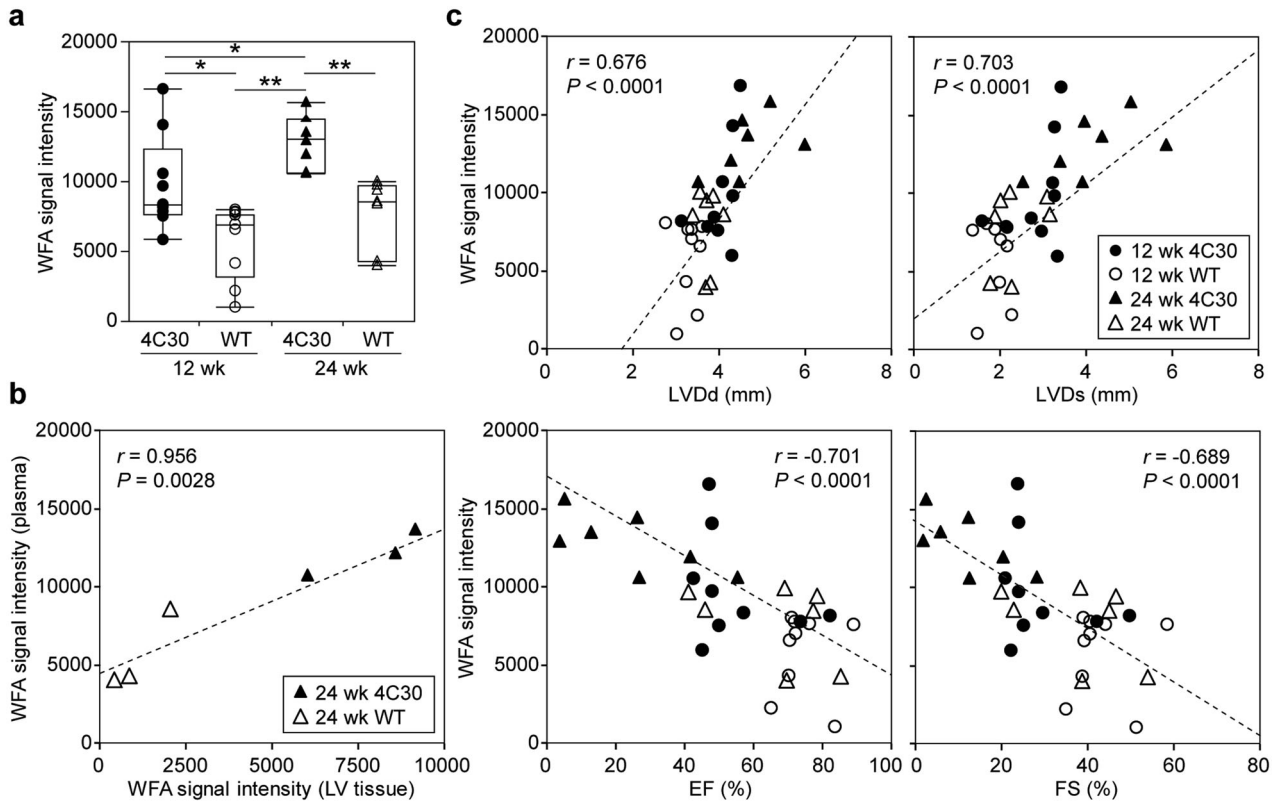

Fig. 7 LMA-based assessment of plasma WFA^+ protein levels. **a** The WFA signal intensities obtained from the LMA analyses of plasma samples from 4C30 and WT mice at 12 weeks (12 wk; $N = 9$ mice/group) or 24 weeks of age (24 wk; $N = 7$ mice/group). Asterisks indicate significant differences between groups (Steel–Dwass test, $^*P < 0.05$, $^{**}P < 0.01$). **b** Correlations of the WFA signal intensities of plasma and LV tissue samples of 24-week-old mice ($N = 3$ mice/group). **c** Correlations of the plasma WFA signal intensities with LV end-diastolic dimension (LVDd), LV end-systolic dimension (LVDs), ejection fraction (EF), and fractional shortening (FS), respectively. Pearson's linear correlation coefficients (r) and P-values are indicated. The LMA data of the LV lysates and plasma samples used for the analyses are presented in Supplementary Tables 7 and 8, respectively

quantification of cardiac fibrosis after myocardial infarction (MI), a predominantly focal type of cardiac fibrosis with scar formation [38]. WGA prefers glycan structures with terminal *N*-acetylglucosamine and sialic acids (Supplementary Table 1), and thereby binds to a broad range of glycoconjugates, including ECM proteins and glycosaminoglycans, such as hyaluronic acid [20]. Since these WGA ligands are present at cell surfaces and interstitial regions of both normal and failing heart tissues, increased WGA staining in fibrotic cardiac tissues can be detected only in cases where the increase in the levels of WGA ligands is significant. Indeed, the WGA staining observed in 4C30 cardiac sections was not specific to fibrotic areas (Fig. 2a), and WGA did not show significantly higher signals in 4C30 hearts than in WT hearts in the LMD–LMA analysis (Fig. 1e). Accordingly, WGA staining cannot be applied to the detection of the diffuse-type fibrosis observed in DCM. In contrast, the levels of WFA ligands (i.e., glycan structures with terminal galactose and *N*-acetylgalactosamine) are low in normal tissues of WT mice, and thus the increased WFA signal in fibrotic cardiac tissues was obviously detectable both in the tissue glycomic profiling (Fig. 1e) and lectin histochemistry (Fig. 2c). Because of these characteristics, the WFA staining method facilitates the detection of the diffuse-type cardiac fibrosis observed in DCM. On the other hand, the WGA staining observed in post MI has some common points with the present WFA staining observed in DCM [38]. First, the distribution and degree of WGA and PSR staining in post-MI hearts were highly correlated. Second, the localization of WGA staining and collagen I in the scar did not overlap. In this context, it would be interesting to evaluate whether WFA staining would also be applicable to the detection and quantification of focal-type cardiac fibrosis, because fibrosis-specific WFA staining is expected to be detected with low background, as demonstrated here.

Although the variations and functions of cardiac ECM constituents in cardiac remodeling have been well investigated [18–20], information on the glycosylation state in failing hearts and disease-related changes in glycan structures is still limited. The present IGOT–LC–MS/MS analyses of $HILIC^+WFA^+$ glycopeptides identified nine

glycosylation sites attached to WFA-binding *N*-glycans of seven WFA^+ ECM proteins (Table 2). Since all these *N*-glycosylation sites have been detected in cardiac tissues of post-MI C57BL/6J mice [39], these sites can also be decorated with WFA^+ *N*-glycans in post-MI fibrotic hearts. In addition, except for one site on Hspg2, all the sites are conserved in orthologous human proteins, suggesting that WFA^+ *N*-glycosylation on these sites may occur in fibrotic cardiac tissues of DCM patients. An important finding was that this WFA^+ *N*-glycosylation was detected mostly on ECM proteins in 4C30 mice. Based on previous proteomic and transcriptomic analyses of LV tissue lysates, none of the identified WFA^+ ECM proteins (Table 2) and WFA^+ ECM *N*-glycoproteins (Supplementary Table 5), except for Postn, showed upregulated expression (a greater than two-fold change) in 4C30 mice compared with that in WT mice [23]. Thus, the present results showing increased levels of WFA^+ ECM proteins in 4C30 hearts suggested that glycosylation was altered in these glycoproteins. Since cardiac ECM proteins are expressed predominantly in, and secreted from, cardiac fibroblasts [9, 18, 40], the present results showing the cooperative altered glycosylation of ECM proteins suggest that the glycosylation machinery was altered in these cells.

Interestingly, a recent study suggested DCM-related glycosylation alteration of Bgn in failing hearts of pediatric and adult patients, in which an additional immunoreactive band was detected around 40 kDa specifically in patients with DCM [41], although the glycosylation has not been verified. Based on another study reporting bands of 38, 45, and 110 kDa corresponding to non-glycosylated, *N*-glycosylated, and *N*-glycan and glycosaminoglycan-attached forms of Bgn, respectively [42], it was likely that the DCM-specific Bgn was the *N*-glycosylated form, consistent with the present results. In addition to Bgn, this study also identified *N*-glycosylation sites with potentially altered *N*-glycans on proteoglycans, including Nid1, Dcn, and Hspg2 (Table 2), highlighting the importance of determining the *N*-glycosylation state of proteoglycans for a better understanding of their functions in the progression of cardiac fibrosis.

Our finding that the levels of WFA^+ glycoproteins were increased in the plasma of DCM mice, according to the degree of cardiac fibrosis, is very interesting because the WFA^+–MAC-2 binding protein glycosylation isoform (M2BPGi) is currently used in clinical practice as a liver fibrosis marker [43, 44]. In addition, serum M2BPGi is also a potential biomarker for idiopathic pulmonary fibrosis [45]. Regarding cardiac diseases, only one study has reported increased M2BPGi levels in patients with chronic heart failure plus abnormal liver function [46]. M2BP is a cell-adhesion ECM protein expressed in numerous organs, including the heart [47]. Since the present results suggest the cooperatively altered glycosylation of ECM proteins, WFA^+–M2BP may also be expressed in fibrotic cardiac tissues, and thereby circulating M2BPGi can be utilized as a cardiac fibrosis marker. M2BP was not identified in WFA^+ fractions in this study, possibly because the majority of cardiac M2BP was secreted into the circulation or lost during perfusion, and the amount of the remaining WFA^+ M2BP was too small for identification, similar to that observed for the proteins identified only as WFA^+ *N*-glycopeptides. In addition, no *N*-glycopeptide of M2BP was identified in WFA^+ glycopeptide fractions, probably because the ring structure of M2BP is fundamental for its WFA-binding ability [43]. Similar to that observed for M2BPGi, WFA can also be employed as a probe for other diseases, including liver cirrhosis, prostate cancer, ovarian cancer, and IgA nephropathy [48], mainly because WFA has low affinity for normal serum glycoproteins; consequently, disease-related WFA^+ glycoproteins can be detected with a high signal/noise ratio [43]. Owing to this situation, the circulating levels of WFA^+ glycoproteins strictly reflected the WFA^+ glycoprotein content in the LV tissues, showing significant correlations with the degree of cardiac remodeling and function (Fig. 7). Accordingly, the circulating levels of the presently identified WFA^+ soluble glycoproteins, which can potentially be measured using WFA–antibody sandwich immunoassays similar to those for M2BPGi [44], are also candidate biomarkers for cardiac fibrogenesis and the associated cardiac remodeling and dysfunction.

This study has several limitations. First, no detailed information was provided on the *N*-glycan structures responsible for the extensive WFA staining of fibrotic cardiac tissues. Second, the identification of WFA^+ proteins and the associated WFA^+ *N*-glycosylation sites in failing hearts was not comprehensive. The glycosylation alteration in WFA-binding proteins should be further investigated in detail, in combination with protein purification methods, such as immunoprecipitation. Finally, the present double-staining analysis detected both WFA^+ Col6a6 and WFA^+ proteins associated with Col6a6, and hence the binding of WFA to proteins cannot be verified by staining analysis alone. The reason why only a small quantity of Col6a6 was stained with WFA remains unclear, but a likely explanation was that WFA binding to WFA^+ *N*-glycans on Col6a6 was hindered by its association with other ECM proteins, as the identified WFA^+ *N*-glycosylation site (Asn^{274}) was located within one of the von Willebrand factor A-like domains responsible for protein–protein associations [36].

In conclusion, the present results of glycomic, glycoproteomic, and histochemical analyses all indicated that WFA staining is a more suitable method for the quantitative assessment of cardiac fibrogenic activity compared with the current collagen staining methods. The results further

suggest that WFA^+ cardiac glycoproteins may be utilized as circulating glyco-biomarkers for the quantification and monitoring of cardiac fibrosis. As cardiac fibrosis is a typical feature of failing hearts in various cardiac diseases, the present findings will facilitate the quantitative assessment of cardiac fibrosis related to these cardiac diseases, including DCM. A next crucial step would be to evaluate whether the fibrosis-specific WFA staining is also observed in failing hearts with other causes, such as ischemia, focusing especially on the differences between diffuse- and focal-type fibrosis and the clinical value of using WFA staining for the monitoring and prognosis of cardiac remodeling and dysfunction.

Acknowledgements We are grateful to Dr. Osamu Suzuki and Dr. Junichiro Matsuda of NIBIOHN for providing 4C30 mice. We thank Dr. Manabu Shirai of NCVC for providing information on mouse cardiac tissue histology. We thank Dr. Yoko Itakura of Tokyo Metropolitan Institute of Gerontology for technical support in tissue section preparation. We also thank Dr. Mika Fujita, Ms. Azusa Tomioka, Ms. Katsue Kiyohara, and Ms. Kozue Hagiwara of AIST for technical assistance. This study was supported by a grant from the Kato Memorial Bioscience Foundation (CNO).

Compliance with ethical standards

Conflict of interest The authors declare that they have no conflict of interest.

References

1. Weintraub RG, Semsarian C, Macdonald P. Dilated cardiomyopathy. Lancet. 2017;390:400–14.
2. Codd MB, Sugrue DD, Gersh BJ, Melton LJ 3rd. Epidemiology of idiopathic dilated and hypertrophic cardiomyopathy. A population-based study in Olmsted County, Minnesota, 1975-1984. Circulation. 1989;80:564–72.
3. Michels VV, Driscoll DJ, Miller FA, Olson TM, Atkinson EJ, Olswold CL, et al. Progression of familial and non-familial dilated cardiomyopathy: long term follow up. Heart. 2003;89:757–61.
4. Halliday BP, Cleland JGF, Goldberger JJ, Prasad SK. Personalizing risk stratification for sudden death in dilated cardiomyopathy. Circulation. 2017;136:215–31.
5. Tayal U, Prasad SK. Myocardial remodelling and recovery in dilated cardiomyopathy. JRSM Cardiovasc Dis. 2017;6: 2048004017734476.
6. Merlo M, Pyxaras SA, Pinamonti B, Barbati G, Di Lenarda A, Sinagra G. Prevalence and prognostic significance of left ventricular reverse remodeling in dilated cardiomyopathy receiving tailored medical treatment. J Am Coll Cardiol. 2011;57:1468–76.
7. Merlo M, Caiffa T, Gobbo M, Adamo L, Sinagra G. Reverse remodeling in dilated cardiomyopathy: insights and future perspectives. Int J Cardiol Heart Vasc. 2018;18:52–57.
8. Kehat I, Molkentin JD. Molecular pathways underlying cardiac remodeling during pathophysiological stimulation. Circulation. 2010;122:2727–35.
9. Kong P, Christia P, Frangogiannis NG. The pathogenesis of cardiac fibrosis. Cell Mol Life Sci. 2014;71:549–74.
10. Weber KT, Pick R, Jalil JE, Janicki JS, Carroll EP. Patterns of myocardial fibrosis. J Mol Cell Cardiol. 1989;21:121–31.
11. Becker MAJ, Cornel JH, van de Ven PM, van Rossum AC, Allaart CP, Germans T. The prognostic value of late gadolinium-enhanced cardiac magnetic resonance imaging in nonischemic dilated cardiomyopathy. JACC Cardiovasc Imaging. 2018;11: 1274–84.
12. Lillie RD. Further experiments with the Masson trichrome modification of Mallory's connective tissue stain. Stain Technol. 1940;15:17–22.
13. Junqueira LC, Bignolas G, Brentani RR. Picrosirius staining plus polarization microscopy, a specific method for collagen detection in tissue sections. Histochem J. 1979;11:447–55.
14. Weber KT. Cardiac interstitium in health and disease: the fibrillar collagen network. J Am Coll Cardiol. 1989;13:1637–52.
15. Rubiś P, Wiśniowska-Śmiałek S, Biernacka-Fijałkowska B, Rudnicka-Sosin L, Wypasek E, Kozanecki A, et al. Left ventricular reverse remodeling is not related to biopsy-detected extracellular matrix fibrosis and serum markers of fibrosis in dilated cardiomyopathy, regardless of the definition used for LVRR. Heart Vessels. 2017;32:714–25.
16. Nabeta T, Inomata T, Iida Y, Ikeda Y, Iwamoto M, Ishii S, et al. Baseline cardiac magnetic resonance imaging versus baseline endomyocardial biopsy for the prediction of left ventricular reverse remodeling and prognosis in response to therapy in patients with idiopathic dilated cardiomyopathy. Heart Vessels. 2014;29:784–92.
17. López B, González A, Ravassa S, Beaumont J, Moreno MU, San José G, et al. Circulating biomarkers of myocardial fibrosis: the need for a reappraisal. J Am Coll Cardiol. 2015;65:2449–56.
18. Louzao-Martinez L, Vink A, Harakalova M, Asselbergs FW, Verhaar MC, Cheng C. Characteristic adaptations of the extracellular matrix in dilated cardiomyopathy. Int J Cardiol. 2016; 220:634–46.
19. Hynes RO, Naba A. Overview of the matrisome—an inventory of extracellular matrix constituents and functions. Cold Spring Harb Perspect Biol. 2012;4:a004903.
20. Rienks M, Papageorgiou A-P, Frangogiannis NG, Heymans S. Myocardial extracellular matrix: an ever-changing and diverse entity. Circ Res. 2014;114:872–88.
21. Suzuki O, Kanai T, Nishikawa T, Yamamoto Y, Noguchi A, Takimoto K, et al. Adult onset cardiac dilatation in a transgenic mouse line with Galβ1,3GalNAc α2,3-sialyltransferase II (ST3Gal-II) transgenes: a new model for dilated cardiomyopathy. Proc Jpn Acad Ser B Phys Biol Sci. 2011;87:550–62.
22. Iwata Y, Ohtake H, Suzuki O, Matsuda J, Komamura K, Wakabayashi S. Blockade of sarcolemmal TRPV2 accumulation inhibits progression of dilated cardiomyopathy. Cardiovasc Res. 2013;99:760–8.
23. Nishigori M, Yagi H, Mochiduki A, Minamino N. Multiomics approach to identify novel biomarkers for dilated cardiomyopathy: proteome and transcriptome analyses of 4C30 dilated cardiomyopathy mouse model. Biopolymers. 2016;106:491–502.
24. Zou X, Yoshida M, Nagai-Okatani C, Iwaki J, Matsuda A, Tan B, et al. A standardized method for lectin microarray-based tissue glycome mapping. Sci Rep. 2017;7:43560.
25. Narimatsu H, Kaji H, Vakhrushev SY, Clausen H, Zhang H, Noro E, et al. Current technologies for complex glycoproteomics and their applications to biology/disease-driven glycoproteomics. J Proteome Res. 2018;17:4097–112.
26. Narimatsu H, Sawaki H, Kuno A, Kaji H, Ito H, Ikehara Y. A strategy for discovery of cancer glyco-biomarkers in serum using newly developed technologies for glycoproteomics. FEBS J. 2010;277:95–105.
27. Nagai-Okatani C, Nagai M, Sato T, Kuno A. An improved method for cell type-selective glycomic analysis of tissue sections

assisted by fluorescence laser microdissection. Int J Mol Sci. 2019;20:700.
28. Kaji H, Yamauchi Y, Takahashi N, Isobe T. Mass spectrometric identification of N-linked glycopeptides using lectin-mediated affinity capture and glycosylation site-specific stable isotope tagging. Nat Protoc. 2006;1:3019–27.
29. Kaji H, Saito H, Yamauchi Y, Shinkawa T, Taoka M, Hirabayashi J, et al. Lectin affinity capture, isotope-coded tagging and mass spectrometry to identify N-linked glycoproteins. Nat Biotechnol. 2003;21:667–72.
30. Sugahara D, Tomioka A, Sato T, Narimatsu H, Kaji H. Large-scale identification of secretome glycoproteins recognized by Wisteria floribunda agglutinin: a glycoproteomic approach to biomarker discovery. Proteomics. 2015;15:2921–33.
31. Togayachi A, Tomioka A, Fujita M, Sukegawa M, Noro E, Takakura D, et al. Identification of poly-N-acetyllactosamine-carrying glycoproteins from HL-60 human promyelocytic leukemia cells using a site-specific glycome analysis method, GlycoRIDGE. J Am Soc Mass Spectrom. 2018;29:1138–52.
32. Nagai-Okatani C, Minamino N. Aberrant glycosylation in the left ventricle and plasma of rats with cardiac hypertrophy and heart failure. PLoS One. 2016;11:e0150210.
33. Gonatas NK, Avrameas S. Detection of plasma membrane carbohydrates with lectin peroxidase conjugates. J Cell Biol. 1973; 59:436–43.
34. Sato T, Tateno H, Kaji H, Chiba Y, Kubota T, Hirabayashi J, et al. Engineering of recombinant Wisteria floribunda agglutinin specifically binding to GalNAcβ1,4GlcNAc (LacdiNAc). Glycobiology. 2017;27:743–54.
35. Härtig W, Brauer K, Brückner G. Wisteria floribunda agglutinin-labelled nets surround parvalbumin-containing neurons. Neuroreport. 1992;3:869–72.
36. Cescon M, Gattazzo F, Chen P, Bonaldo P. Collagen VI at a glance. J Cell Sci. 2015;128:3525–31.
37. Lee YC, Kojima N, Wada E, Kurosawa N, Nakaoka T, Hamamoto T, et al. Cloning and expression of cDNA for a new type of Gal beta 1,3GalNAc alpha 2,3-sialyltransferase. J Biol Chem. 1994;269:10028–33.
38. Emde B, Heinen A, Gödecke A, Bottermann K. Wheat germ agglutinin staining as a suitable method for detection and quantification of fibrosis in cardiac tissue after myocardial infarction. Eur J Histochem. 2014;58:2448.
39. Tian Y, Koganti T, Yao Z, Cannon P, Shah P, Pietrovito L, et al. Cardiac extracellular proteome profiling and membrane topology analysis using glycoproteomics. Proteomics Clin Appl. 2014;8: 595–602.
40. Ivey MJ, Tallquist MD. Defining the cardiac fibroblast. Circ J. 2016;80:2269–76.
41. Jana S, Zhang H, Lopaschuk GD, Freed DH, Sergi C, Kantor PF, et al. Disparate remodeling of the extracellular matrix and proteoglycans in failing pediatric versus adult hearts. J Am Heart Assoc. 2018;7:e010427.
42. Barallobre-Barreiro J, Baig F, Fava M, Yin X, Mayr M. Glycoproteomics of the extracellular matrix: a method for intact glycopeptide analysis using mass spectrometry. J Vis Exp. 2017; https://doi.org/10.3791/55674
43. Kuno A, Ikehara Y, Tanaka Y, Ito K, Matsuda A, Sekiya S, et al. A serum "sweet-doughnut" protein facilitates fibrosis evaluation and therapy assessment in patients with viral hepatitis. Sci Rep. 2013;3:1065.
44. Narimatsu H. Development of M2BPGi: a novel fibrosis serum glyco-biomarker for chronic hepatitis/cirrhosis diagnostics. Expert Rev Proteomics. 2015;12:683–93.
45. Kono M, Nakamura Y, Oyama Y, Mori K, Hozumi H, Karayama M, et al. Increased levels of serum Wisteria floribunda agglutinin-positive Mac-2 binding protein in idiopathic pulmonary fibrosis. Respir Med. 2016;115:46–52.
46. Okada A, Kanzaki H, Hamatani Y, Takashio S, Takahama H, Amaki M, et al. Increased serum Wisteria floribunda agglutinin positive Mac-2 binding protein (Mac-2 binding protein glycosylation isomer) in chronic heart failure: a pilot study. Heart Vessels. 2018;33:385–92.
47. Sasaki T, Brakebusch C, Engel J, Timpl R. Mac-2 binding protein is a cell-adhesive protein of the extracellular matrix which self-assembles into ring-like structures and binds beta1 integrins, collagens and fibronectin. EMBO J. 1998;17: 1606–13.
48. Narimatsu H, Sato T. Wisteria floribunda agglutinin positive glycobiomarkers: a unique lectin as a serum biomarker probe in various diseases. Expert Rev Proteomics. 2018;15:183–90.